Supplementary Information

Stability Assessment of HKUST-1 Metal-Organic Framework with Gold Nanoparticles

Hudson B. da Silva,[a] Flavia H. e Silva,[b] Natália Regina de S. Araújo,[c] Maria Betânia F. Marques,[c,d] Rita de Cássia O. Sebastião,[c] Charlane C. Corrêa*,[b] and Gustavo F. S. Andrade*,[a]

[a]*Laboratório de Nanoestruturas Plasmônicas (LabNano), Departamento de Química, Instituto de Ciências Exatas (ICE), Universidade Federal de Juiz de Fora (UFJF), 36036-900 Juiz de Fora-MG, Brazil*

[b]*Grupo de Pesquisa em Química dos Materiais Porosos (GPQMAP), Departamento de Química, Instituto de Ciências Exatas (ICE), Universidade Federal de Juiz de Fora (UFJF), 36036-900 Juiz de Fora-MG, Brazil*

[c]*Departamento de Química, Instituto de Ciências Exatas (ICEx), Universidade Federal de Minas Gerais (UFMG), 31270-901 Belo Horizonte- MG, Brazil*

[d]*Faculdade de Ciências Farmacêuticas (FCF), Universidade Federal de Alfenas (UFAL), 37130-001 Alfenas-MG, Brazil*

*e-mail: charlane.cimini@ufjf.br; gustavo.andrade@ufjf.br

Hudson Batista da Silva: https://orcid.org/0000-0001-9240-3525
Flavia Heredia e Silva: https://orcid.org/0009-0005-8922-8515
Natália Regina de Souza Araújo: https://orcid.org/0000-0001-9138-6284
Maria Betânia Freitas Marques: https://orcid.org/0000-0002-0561-2343
Rita de Cássia Oliveira Sebastião: https://orcid.org/0000-0002-5158-7783
Charlane Cimini Corrêa: https://orcid.org/0000-0002-7113-8870
Gustavo F. S. Andrade: https://orcid.org/0000-0003-0718-9400

Figure S1 shows the PXRD diffractograms of HKUST-1 modified with AuNP-Cit and AuNP-Boron, both by the post-synthesis method (PSM) and by the *in situ* method in the 5-50º (2θ) range, and magnification of the region between 35 and 50º allows observation of additional reflections attributed to metallic gold, confirming the presence of nanoparticles in the modified material.

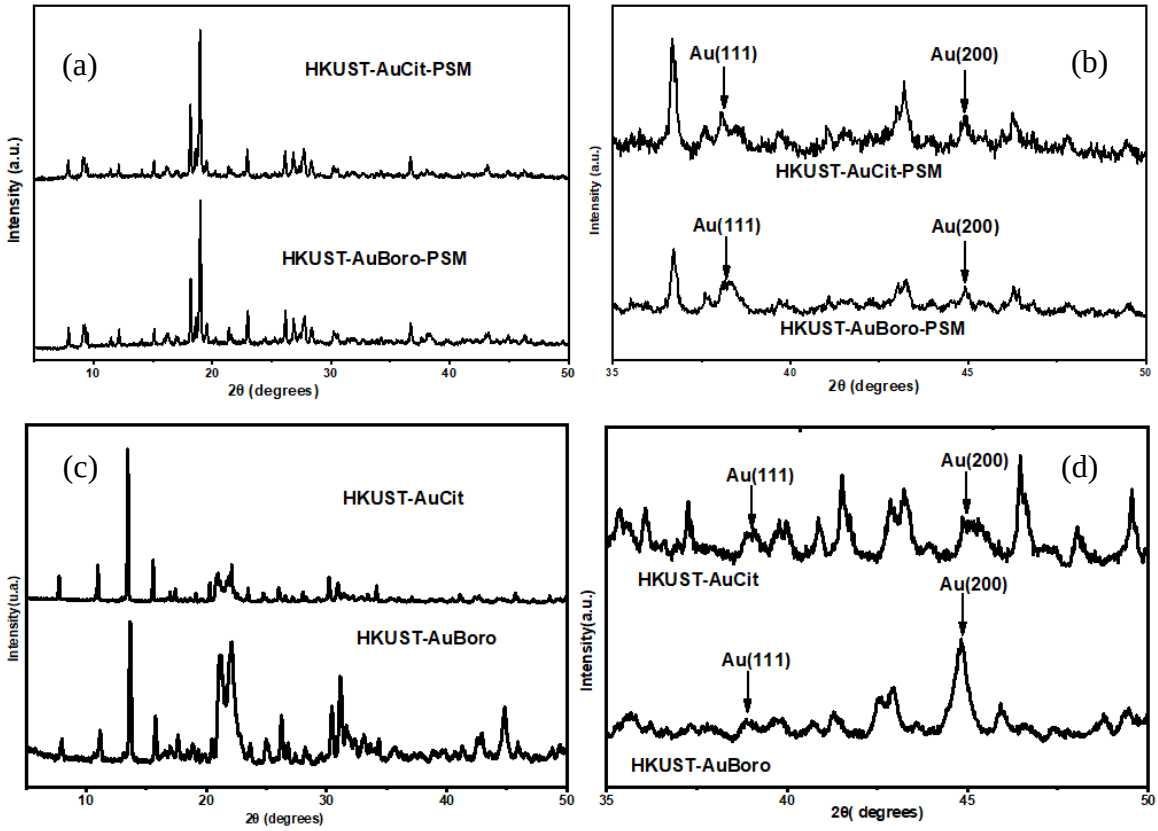

Figure S1. Powder X-ray diffraction patterns (PXRD, λ = 1.78897 Å) of HKUST-1 modified by the post-synthesis method (PSM) in the 5-50° 2θ range (a) and in the 35-50º 2θ range (b), highlighting the peaks associated with gold. The PXRD patterns of HKUST-1 modified by the *in situ* method in the 5-50º 2θ range (c) and in the 35-50º 2θ range (d) also enhance the reflections attributed to gold.

Figure S2 shows the EDS spectra comparing the AuNP-modified samples. It can be seen that all the spectra show the typical peaks of HKUST-1, related to the constituent elements of the MOF (Cu, C, and O). In addition, the EDS spectra of the modified HKUST-1 showed additional peaks attributed to gold, indicating the presence of the nanoparticles. In contrast to pure HKUST-1, all modified samples show additional peaks corresponding to Au, indicating the presence of gold nanoparticles in the MOF structure.

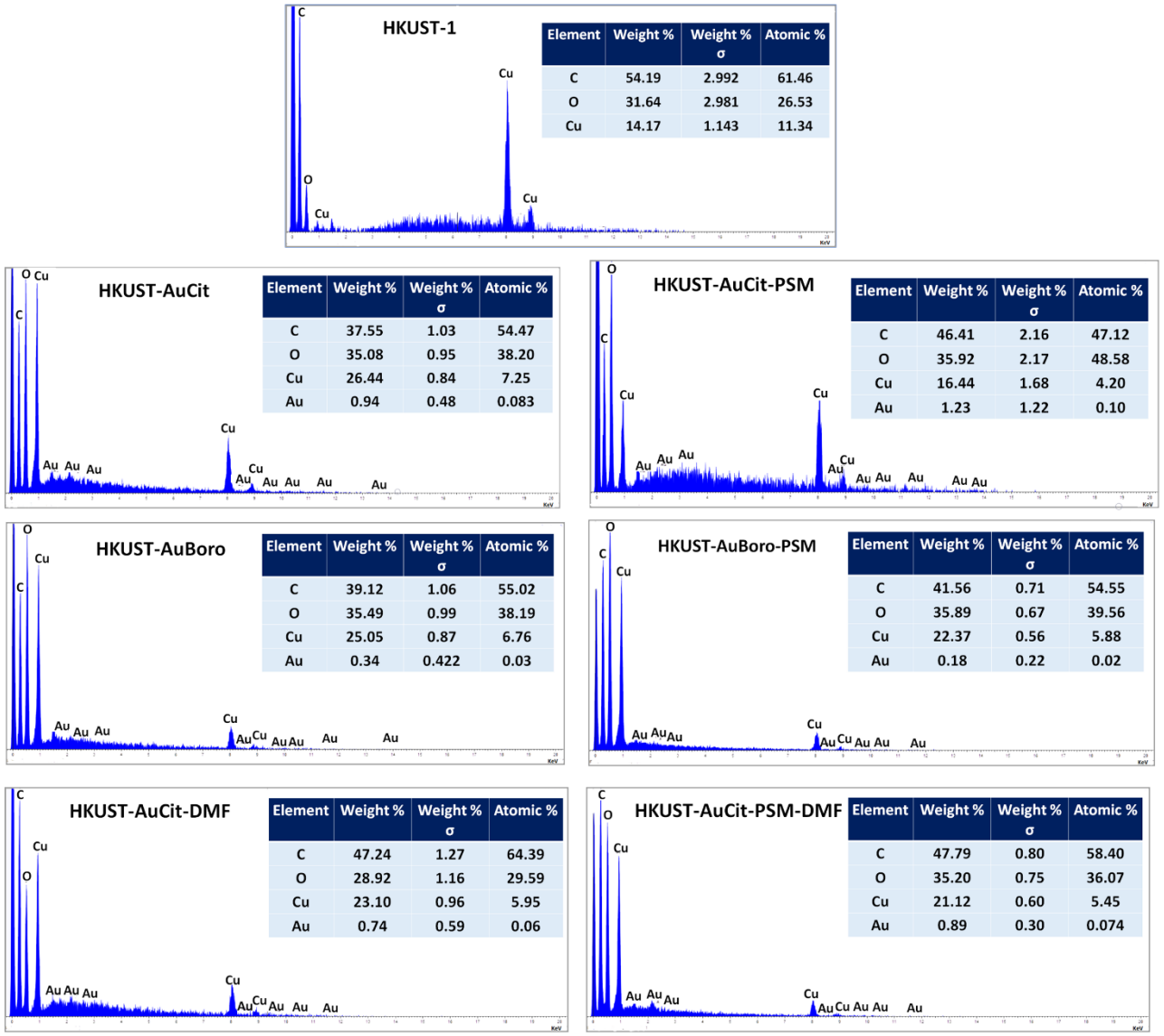

Figure S2. EDS spectra of HKUST-1 samples doped with gold nanoparticles (AuNP) by different methods.

Figure S3 shows the elemental distribution maps obtained by EDS for the pure HKUST-1 sample and for the materials modified with gold nanoparticles (AuNPs), prepared by different synthesis and post-modification strategies. For all samples, the homogeneous presence of the elements carbon (C), oxygen (O), and copper (Cu) is observed, confirming the preservation of the chemical composition characteristic of the HKUST-1 MOF structure after the modification processes. In the modified materials, EDS maps show the successful entry of AuNPs, distributed evenly and homogeneously on the surface of HKUST-1.

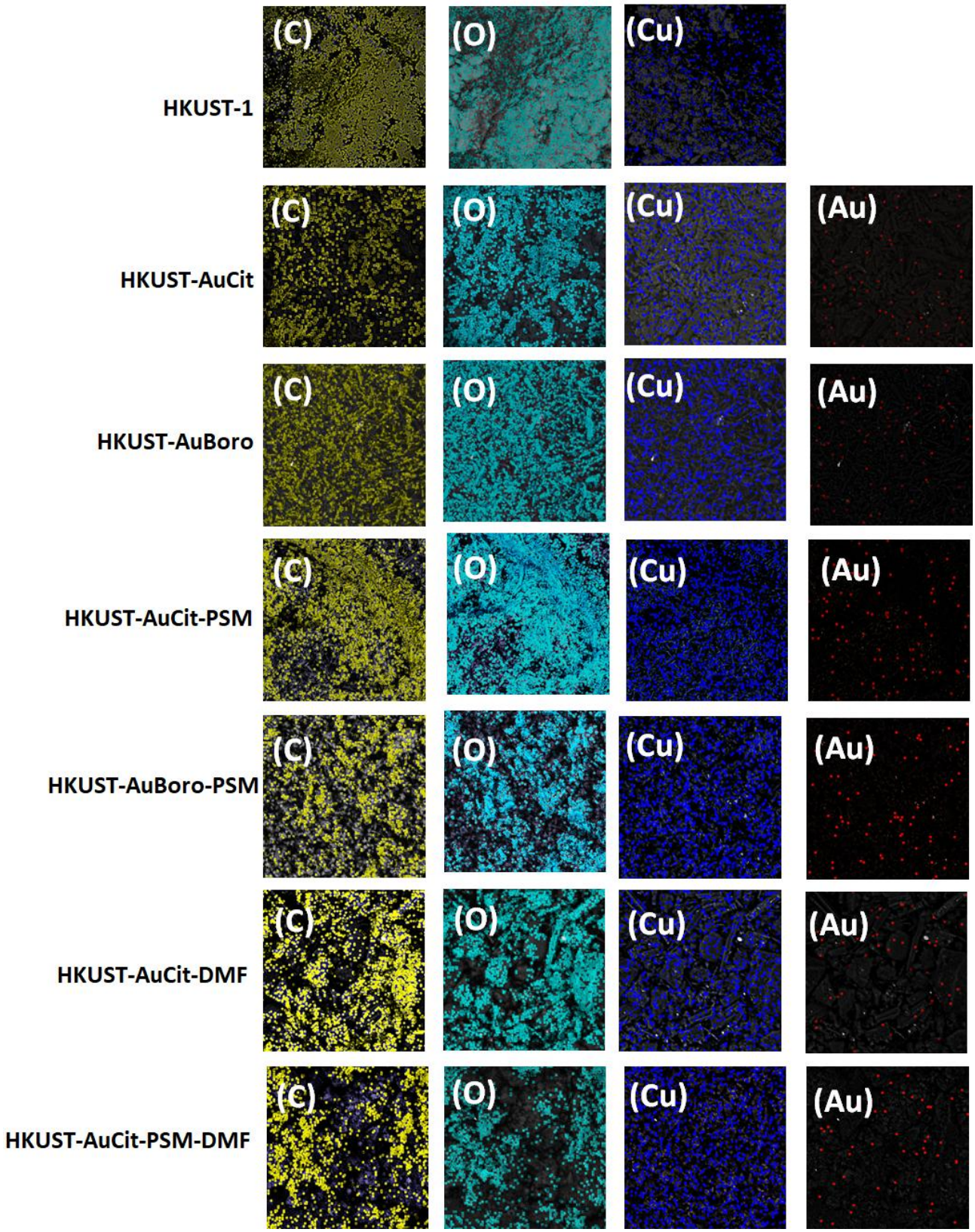

Figure S3. EDS element mapping analysis of HKUST-1 samples doped with gold nanoparticles (AuNP) by different methods.

The UV-Vis-NIR diffuse reflectance technique was employed to assess the presence of AuNPs in the HKUST-1 structure. Figure S4 shows the reflectance spectra of pure HKUST-1 and the samples modified *in situ* and by the post-synthesis method with AuNP-Boro (Figure S4a) and AuNP-Cit (Figure S4b) nanoparticles. In the spectra of HKUST-

AuCit and HKUST-AuCit-PSM, an additional reflectance band at 540 nm was identified, which can be attributed to the plasmon extinction of the AuNP; a similar observation was possible for HKUST-AuBoro and HKUST-AuBoro-PSM. This band in the UV-Vis-NIR can be regarded as a strong indication of the presence of AuNP nanoparticles in the structure of modified HKUST-1; no structural changes could be identified considering these analyses. The intense and broad band at 540 nm was also observed in the HKUST-1 regenerated with ethanol after post-synthesis modification (Figure S4c) and *in situ* (Figure S4d) with AuNP-Cit. A similar result was obtained for HKUST-1 modified with AuCit-DMF, as shown in Figure S4e.

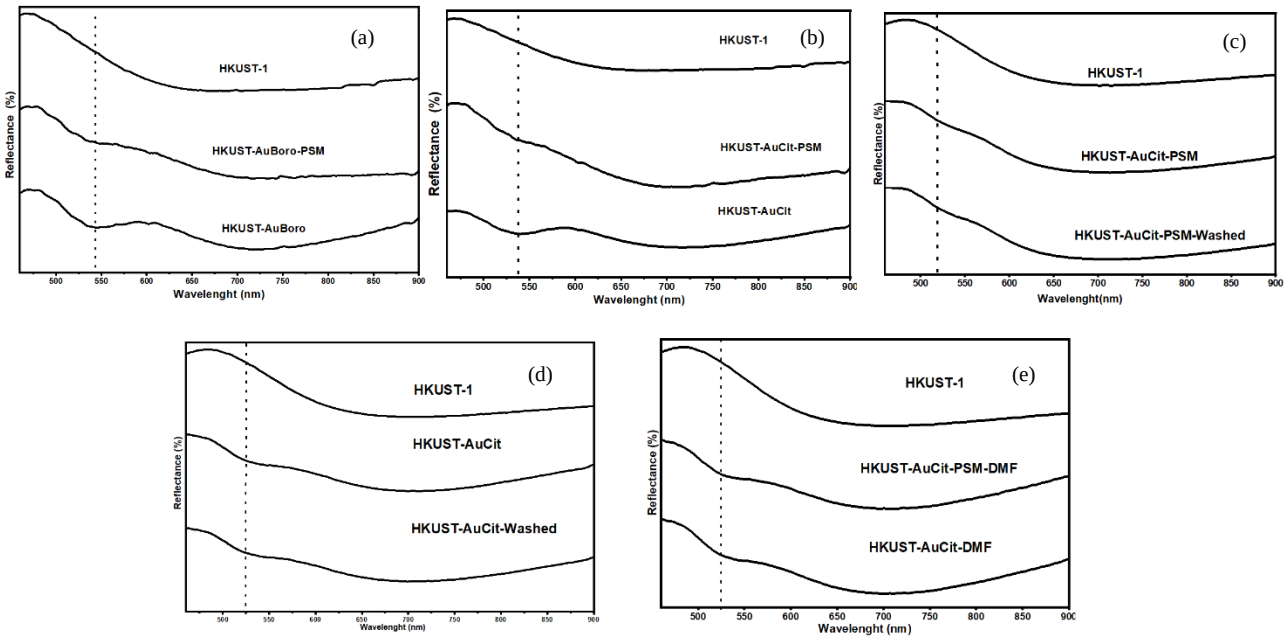

Figure S4. UV-Vis diffuse reflectance spectra comparing HKUST-1 with HKUST-1 modified in situ and post-synthesized with nanoparticles (a) AuNP-Boro and with (b)AuNP-Cit. (c) Spectra obtained for HKUST-1 regenerated with ethanol after post-synthesis modification (c), in situ (d) with AuNP-Cit. (e) Spectra obtained for HKUST-1 modified with AuNP-Cit-DMF.

Figure S5a shows the UV-Vis spectra obtained for AuNP-Cit and AuNP-Cit-DMF. After changing the dispersing medium, there was a slight change in the maximum extinction of the plasmonic band and aggregation, but the nanoparticles remained stable. Figure S5b shows the UV-Vis spectrum obtained for the AuNP-Boro nanoparticle.

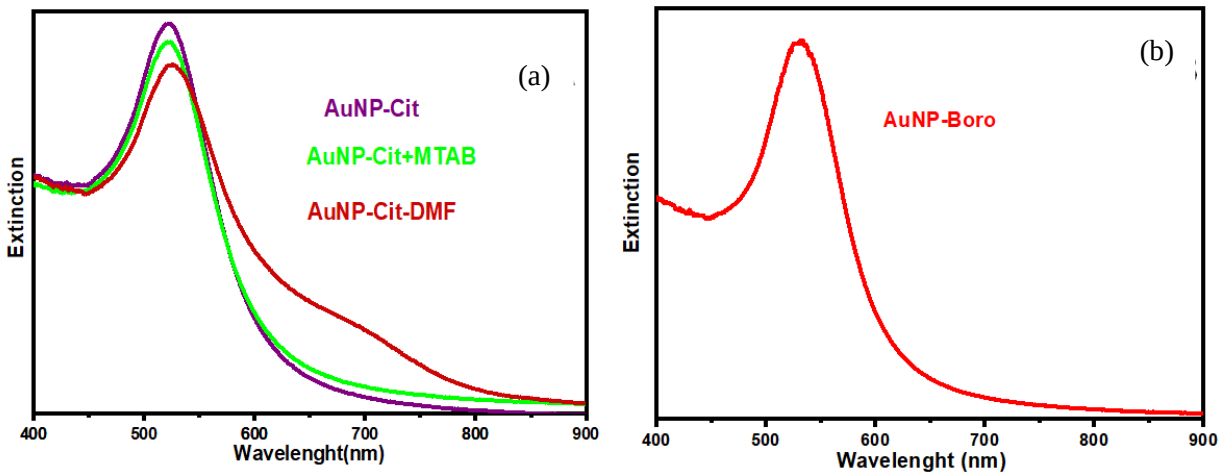

Figure S5. (a) UV-Vis spectra comparing the colloidal suspensions of AuNP-Cit, AuNP+MTAB and AuNP-Cit-DMF, and (b) UV-Vis spectra of colloidal suspensions of AuNP-Boro.

Tables S1, S2, and S3 show, respectively, the tentative assignment of the main vibrational modes of pure HKUST-1, HKUST-1 modified by the *in situ* method, and HKUST-1 modified by the PSM method with gold nanoparticles.[1-3]

Some of the main bands identified in the spectrum are recorded in the tables, such as the band at 1006 cm^{-1} attributed to the ring breathing mode that appears at 1025 cm^{-1} in the spectrum of the gold-containing MOF.

Table S1. Attempted assignment of the main active vibrational modes in the Raman and infrared spectra (FTIR) for HUKUST-1

Raman / cm^{-1}	FTIR / cm^{1}	Assignment
1605	1625	νCC
1580	1573	νCC
1460	1445	ν_{as} COO^{-}
1365	1382	ν_{s} COO^{-}
1200	–	δC–H
1006	–	ν_{s} $(C=C)_{ring}$
–	1117	δC–H
820	726-752	βC–H
–	480	ν (Cu–O)
280	–	$\nu(Cu–O_{water})$
173-191	–	ν(Cu–Cu)

ν: stretching; ν_s: symmetric stretching; ν_{as}: asymmetric stretching, δ: in-of-plane bending; β: out-of-plane bending.

Table S2. Attempt to assign the main active vibrational modes in the Raman and infrared spectra (FTIR) for modified HUKUST-1 using the *in situ* method

Raman / cm^{-1}	FTIR / cm^{1}	Assignment
1630	–	νCC
1610	1615	νCC
–	1562	νCC
1460	1446	ν_{as} COO^{-}
–	1382	ν_{s} COO^{-}
1200	–	δC–H
1025	–	ν_{s} $(C=C)_{ring}$
–	1117	δC–H
820	726-752	γC–H
–	480	ν (O–Cu–O)
264	–	$\nu(Cu–O_{water})$
173-191	–	ν(Cu–Cu)

ν: stretching; ν_s: symmetric stretching; ν_{as}: asymmetric stretching, δ: in-of-plane bending; β: out-of-plane bending.

Table S3. Attempt to assign the main active vibrational modes in the Raman and infrared spectra (FTIR) for modified HUKUST-1 using the PSM method

Raman / cm^{-1}	FTIR / cm^{1}	Assignment
1630	–	νCC
1610	1615	νCC
–	1562	νCC
1460	1446	ν_{as} COO^{-}
–	1382	ν_{s} COO^{-}
1200	–	δC–H
1025	–	ν_{s} $(C=C)_{anel}$
–	1117	δC–H
820	726-752	γC–H
–	480	ν (O–Cu–O)
264	–	$\nu(Cu–O_{water})$
191	–	ν(Cu–Cu)

ν: stretching; ν_s: symmetric stretching; ν_{as}: asymmetric stretching, δ: in-of-plane bending; β: out-of-plane bending.

The zeta potential results shown in Figure S6, along with the size distribution profiles obtained by DLS presented in Figure S7, provide important information about the colloidal stability and dispersion behavior of the synthesized gold nanoparticles (AuNPs). All samples exhibited negative zeta potential values.

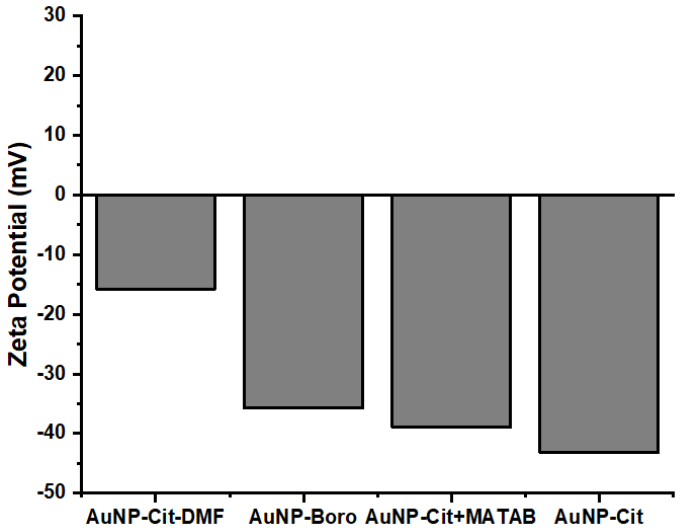

Figure S6. ζ-potential of AuNP-Cit, AuNP + MTAB, AuNP-Cit-DMF and AuNP-Boro.

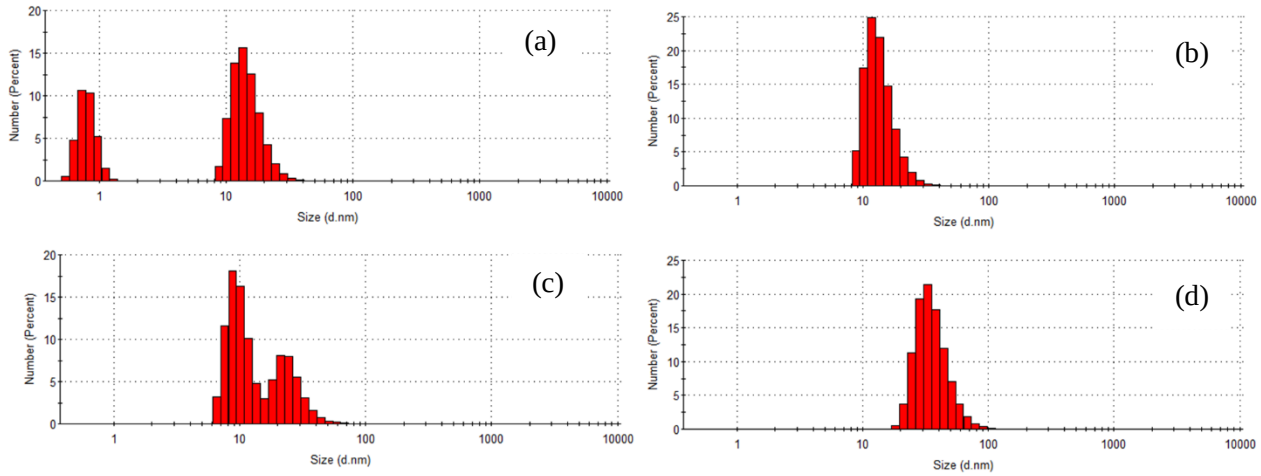

Figure S7. DLS intensity hydrodynamic diameter (d,nm) distribution histograms for (a) AuNP-Cit, (b) AuNP+MTAB, (c) AuNP-Cit-DMF and (d) AuNP-Boro.

Figure S8 shows a comparison between the XRD patterns of the modified HKUST-1 samples and the diffraction patterns of the MOF precursors, trimesic acid and copper(II) nitrate salt, along with copper(II) oxide, which was included to check for the possible presence of degradation products within the structure after modification with AuNP. No characteristic peaks associated with these compounds were observed in the diffractograms of the modified HKUST-1 samples in Figure S8.

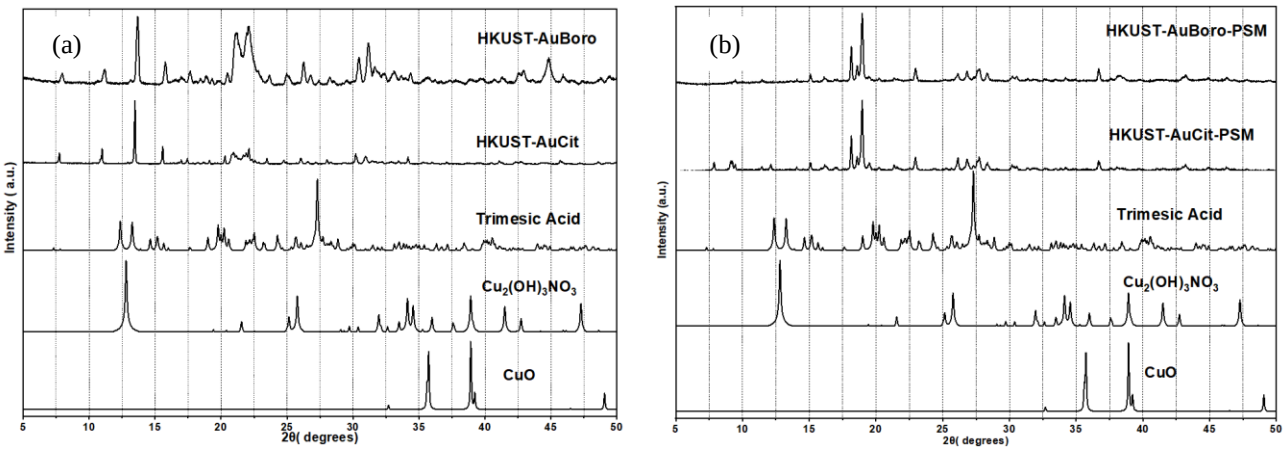

Figure S8. Comparison of the standard X-ray diffraction patterns of trimesic acid, copper(II) nitrate trihydrate, and copper(II) oxide with those of the samples modified in situ (a) and those modified via post-synthetic modification (b).

Figure S9 shows TG/DTA curves at 10 °C min^{-1} for all samples. The data are represented by TG curve (red lines), DTA curve (green lines), temperature (blue lines), and DTG (pink lines). Mass changes and temperature differences between the sample and reference indicate heat-induced phase transitions. The temperature range of each phenomenon was confirmed by the inflection of the TG curves' first derivative (DTG). All samples showed a gradual mass loss (Δm 19-29%) at the beginning of the analysis, ca. 30 ºC, as observed in the TG curves, and exhibit a thermal stability close to 287 ºC. It should be noted that the modification of the HKUST-AuCit PSM and HKUST-AuBoro PSM samples resulted in a slight increase in thermal stability (up to 291 ºC). From this point, thermal decomposition occurs (Δm 43-50%) with an intense exothermic phenomenon (5.81-7.18 kJ g^{-1}) observed in the DTA curves, which caused an increase in the

temperature of the equipment. This exothermic event was not considered to calculate the thermal decomposition kinetics of each sample from the TG curve data. Instead, an interpolated temperature curve was considered solely in this region.

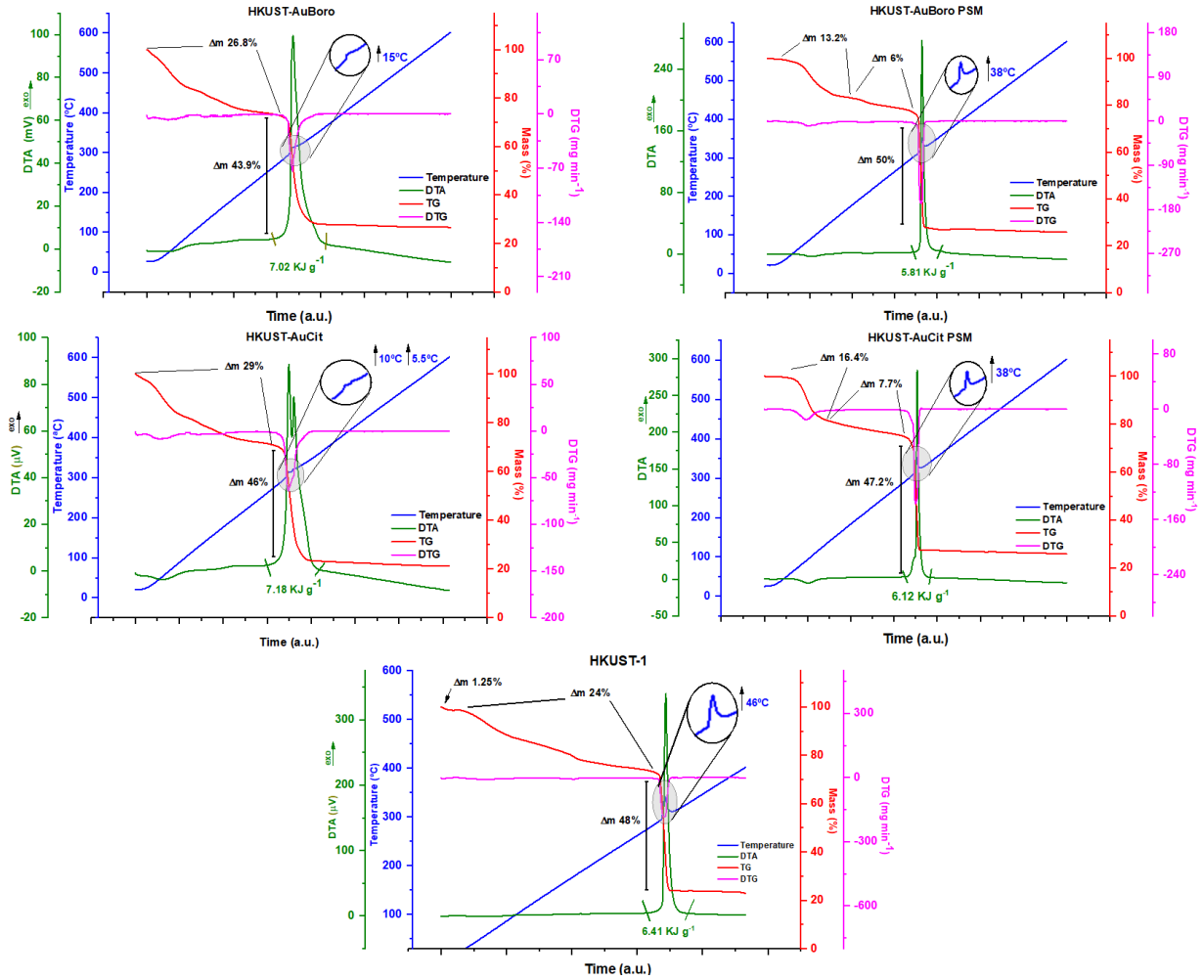

Figure S9. Thermal behavior of HKUST-1, HKUST-AuCit, HKUST-AuBoro, HKUST-AuCit PSM and HKUST-AuBoro PSM. Data are represented by temperature (blue lines), differential thermal analysis - DTA curve (green lines), thermogravimetry - TG curve (red lines) and derivative thermogravimetry - DTG (pink lines).

Figure S10 presents the E_a and the logarithm of the frequency factor (ln A) for all HKUST samples. The decreasing E_a behavior indicates that the remaining solid product should require less energy to degrade from this stage. The mean E_a for HKUST-1 was lower than the values for the materials with AuNP added. The greatest increase was observed with the addition of AuCit. The value for HKUST-1 was 123 kJ mol^{-1}. For HKUST-AuCit and HKUST-AuCit-PSM, E_a was 161 kJ mol^{-1} for both samples. For HKUST-AuBoro and HKUST-AuBoro-PSM the values were 142 and 138 kJ mol^{-1}, respectively. These results indicate that a catalytic event occurs during degradation. The same pattern occurs for the frequency factor.

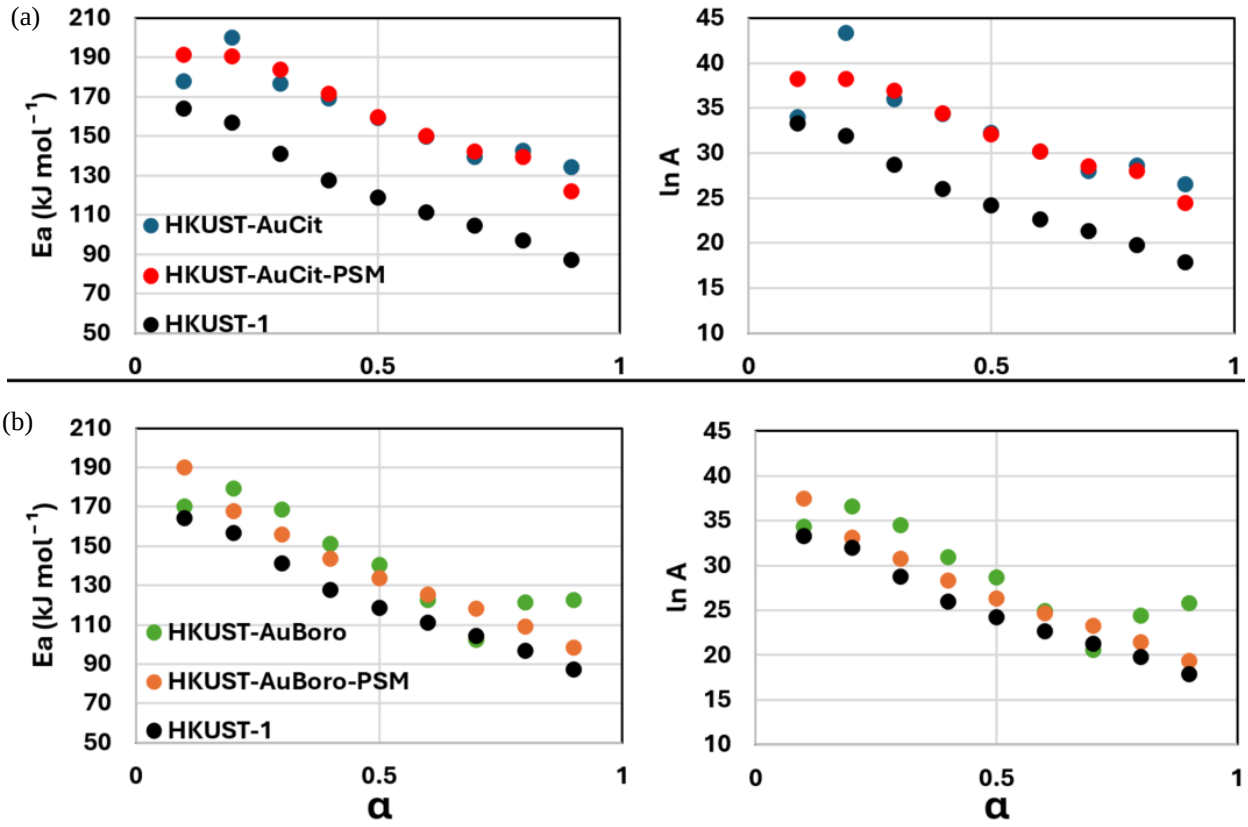

Figure S10. Activation energy (E_a) and logarithm of the frequency factor (lnA) for the thermal decomposition process of HKUST samples.

The contribution of the models calculated by the MLP network is shown in Figure S11. The Avrami-Erofeev with order n = 2 is the kinetic model that contributes most in all samples, indicating that the decomposition starts at nucleation sites, followed by diffusion of low molecular weight volatiles. The nucleation sites are probably imperfections in the octahedral structure. Adding AuNP does not seem to have interfered with the physical mechanism by which HKUST-1 undergoes degradation. In general, the proportion of the contribution is similar in the first-order kinetic model (F1) and Avrami-Erofeev (Am) with order n = 1.5 to 3, even more for the PSM samples.

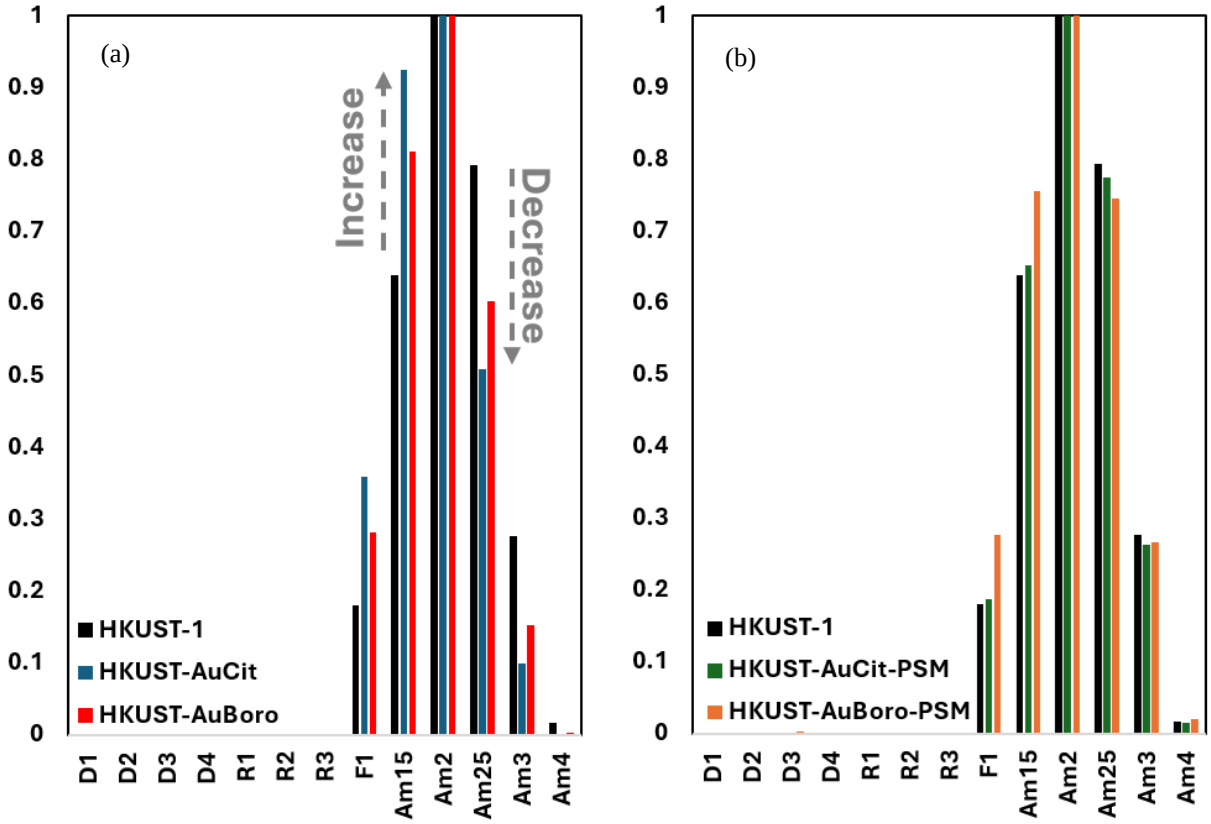

Figure S11. Thermal decomposition process contribution model for HKUST samples calculated by MLP network for: HKUST-1, HKUST-AuCit, and HKUST-AuBoro (a); HKUST-1, HKUST-AuCit-PSM, and HKUST-AuBoro-PSM (b).

Figure S12 shows infrared spectra (FTIR) comparing pure HKUST-1 with samples modified with AuNP-Cit by the in situ and PSM methods, before and after ethanol washing processes. No relevant changes were observed after washing the AuNP-modified HKUST-1. There was an improvement in the signal-to-noise ratio of the spectra, which can be attributed to the removal of water molecules coordinated to the structure. For the MOF modified by the PSM process, there was an improvement in the resolution of the bands after washing with ethanol; the bands at 726 and 752 cm^{-1} were attributed to out-of-plane angular deformation of C–H bonds.

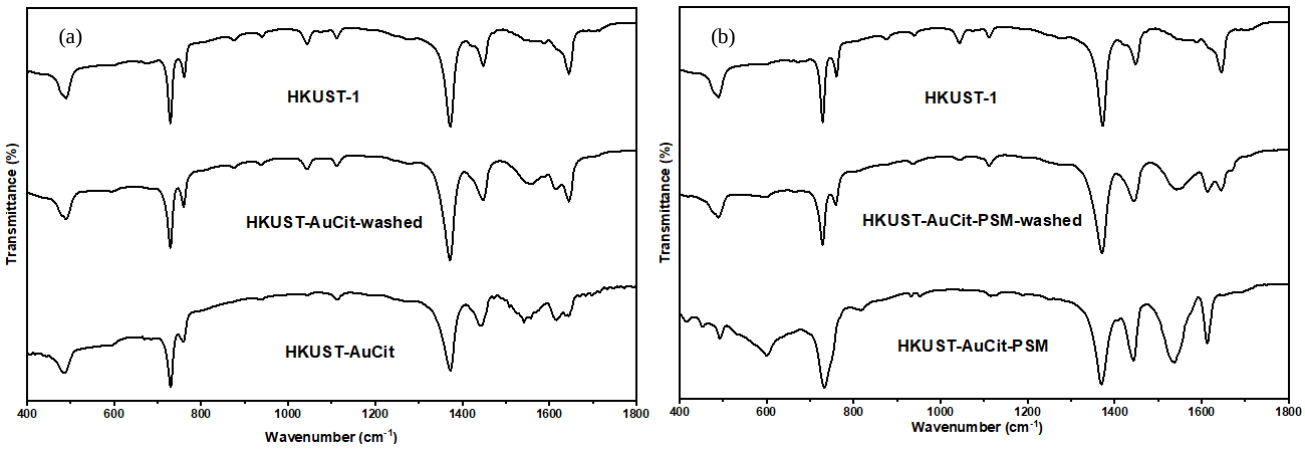

Figure S12. FTIR spectra acquired using the ATR method comparing HKUST-1 before and after association with gold nanoparticles. (a) Spectra of HKUST-1, HKUST-AuCit, and HKUST-AuCit-washed. (b) Spectra of HKUST-1, HKUST-AuCit-PSM, and HKUST-AuCit-PSM-washed.

References

1. Gentile, F. S.; Pannico, M.; Causà, M.; Mensitieri, G.; Di Palma, G.; Scherillo, G.; Musto, P.; *J. Mater. Chem. A Mater.* **2020**, *8*, 10796. [Crossref]
2. Dhumal, N. R.; Singh, M. P.; Anderson, J. A.; Kiefer, J.; Kim, H. J.; *J. Phys. Chem. C* **2016**, *120*, 3295. [Crossref]
3. Todaro, M.; Alessi, A.; Sciortino, L.; Agnello, S.; Cannas, M.; Gelardi, F. M.; Buscarino, G.; *J. Spectrosc.* **2016**, *2016*, ID 8074297. [Crossref]